Solid-State Microcellular Acrylonitrile-Butadiene-Styrene Foams

Ross E. Murray, John E. Weller and Vipin Kumar*

Department of Mechanical Engineering, Box 352600,
University of Washington, Seattle, Washington, 98195, USA

SUMMARY

Microcellular ABS foams are a novel family of materials with the potential to significantly reduce material costs in a number of applications that currently use solid polymer. ABS foams were produced using carbon dioxide in a solid-state process. Solubility and diffusivity of CO_2 in ABS was measured, and the latter was found to depend significantly on the gas concentration. The useful range of process-space for ABS-CO_2 was characterized. Closed cell ABS foams were produced with densities ranging from 1.03 g/cm^3 (almost completely solid) to 0.09 g/cm^3. It was determined that there are many different processing conditions that can produce microcellular ABS foams that have the same density. The cell nucleation density was of the order of 10^{11} cells per cm^3, and the average cell sizes observed ranged from 0.5 µm to 5.6 µm.

INTRODUCTION

ABS (Acrylonitrile-butadiene-styrene) has grown to become one of the most widely used thermoplastic in the world because of the wide range of available properties, ease of processing, and a good balance between price and performance[1]. ABS is an amorphous copolymer alloy, with acrylonitrile bringing chemical resistance and heat stability, butadiene bringing toughness, and styrene providing good processing characteristics. These qualities provide an excellent engineering thermoplastic that is used for a wide range of products, including computer housings, automotive interiors, appliances, and building materials. In many applications, the solid ABS can be replaced by relatively high density microcellular foams, since the properties of solid ABS are not fully utilized. Currently, the only process than can produce foams suitable for thin cross-sections is the solid-state microcellular process originally developed at MIT as a way to

---

*Corresponding author. E-mail address: vkumar@u.washington.edu

---

produce high strength polymer foams which can reduce the amount of material used in manufactured products[2]. This process produces foams with a very large number of very small cells, typically on the order of 10 μm diameter, and thus the phase "microcellular foams" was coined.

The batch microcellular process has two stages. In the first stage a thermoplastic sample is placed in a pressure vessel which is then pressurized with a non-reacting gas. Carbon dioxide and nitrogen are typically used as the foaming agents because of their low cost and high solubility in most polymers. The polymer sample absorbs the gas until an equilibrium gas concentration is reached. At this point, the sample is removed from the pressure vessel. In the second stage of the microcellular process the sample is heated, typically in a hot bath, to induce foaming. The temperature of the hot bath is in the neighbourhood of the glass transition temperature of the polymer, and thus the polymer remains in a solid, or rubbery state, well below the melting point, during the entire process. To distinguish these foams from the common foams made from polymer melts, they are described as "solid state" foams.

The process described above is a batch process used to produce relatively small amounts of foam specimens at a time. The production capability of the solid-state microcellular foams has increased with the development of the semi-continuous process[3,4]. In the semi-continuous process the sheet of polymer placed in the pressure vessel is replaced with a roll of polymer which has a gas permeable material rolled up in it to allow gas to diffuse into the entire surface of the roll. The polymer roll and gas permeable material are first separated, and then the polymer sheet is drawn through a hot bath to foam, and a cold bath if necessary to quench the structure.

Microcellular foams can be produced with a wide range of densities and with an integral skin[5]. Due to their potential as a novel family of materials, a number of polymer-gas systems have been explored in recent years, including polystyrene, polycarbonate, PET, PETC, and PVC[6-12]. In this paper we present a detailed experimental characterization of the ABS-CO_2 system, and explore the effects of key process parameters on the microstructure.

EXPERIMENTAL

Commercially available Cycolac GPX 3700 ABS, manufactured by General Electric was used in this study. All of the specimens were produced from 1.5 mm thick sheet with natural colour. The unprocessed material has a density of 1.04 g/cm^3, and a glass transitions temperature of about 116°C.

Solubility and diffusivity measurements

Specimens were cut from 1.5 mm thick sheet to dimensions of 2.5 x 2.5 cm. Each sample was then saturated in a pressure vessel at 26.7°C (80°F) controlled to ±1°C. The temperature and pressure used to saturate the specimens will be referred to as the saturation temperature and saturation pressure respectively. The saturation pressure was controlled to within ±35 kPa (± 5 psi). The samples were periodically removed from the pressure vessel and weighed on a precision balance with accuracy of ±10 µg to determine the amount of gas absorbed. Because the amount of gas absorbed by the samples was on the order of 10 mg, this method provided sufficient accuracy.

Desorption measurements were made from fully saturated samples. After reaching equilibrium CO_2 concentration, the samples were allowed to desorb the CO_2 while held at 26.7°C (80°F) and atmospheric pressure. During the desorption experiments, the samples were weighed on a precision balance to determine the remaining CO_2 concentration.

Foam sample preparation and characterization

Samples were cut to dimensions of 2.5 cm x 2.5 cm and saturated in a pressure vessel maintained at 26.7 ± 1°C (80°F) until an equilibrium CO_2 concentration was reached. The time required to reach equilibrium was determined from the sorption measurements discussed above. After saturation, all specimens were allowed to desorb gas for five minutes prior to foaming. The same desorption time, 5 minutes, was used for all specimens to ensure that the integral unfoamed skin thickness was negligibly small. After desorption, the samples were foamed by heating in a glycerin bath for a length of time that will be referred to as the foaming time. The temperature of the glycerin bath used to foam the specimens will be referred to as the foaming temperature. All samples were foamed for five minutes. Once the foaming time had elapsed, the foamed specimens were immediately quenched in a water bath maintained at room temperature. Specific values of the saturation pressures, foaming temperatures, and foaming times will be discussed later. After foaming, the samples were immersed in liquid nitrogen and then fractured to expose the internal microstructure. The fractured surfaces were made conductive by deposition of Au-Pd vapour and then studied under a scanning electron microscope (SEM). All SEM micrographs were taken along the centre-line of the sample.

Determination of cell size and cell nucleation density

The average cell size, cell size distribution, and number of bubbles per unit volume of foam were determined by Saltikov's method described in detail by Underwood[13]. Saltikov's method allows the characteristics of a three dimensional distribution of spheres to be estimated from a two dimensional image, such as a micrograph. Previously it was assumed that the fracture plane passed through the centre of all bubbles in a micrograph, introducing a small error in the estimation of the average cell size, cell size distribution, and cell nucleation density. In addition, it was also assumed previously that the number of bubbles per unit volume (i.e. bubble density) could be determined by cubing the line density. Saltikov's method provides a more robust procedure for estimating the bubble density, and is applicable to a wider range of microstructures. Saltikov's method was implemented by digitizing an SEM micrograph with approximately 200 bubbles, and using NIH Image to determine the areas of the bubbles. NIH Image is a public domain image processing and analysis program developed at the Research Services Branch (RSB) of the National Institute of Mental Health (NIMH), part of the National Institutes of Health (NIH). The mean bubble diameter and standard deviations reported in this paper are based on the lognormal distribution proposed by Saltikov.

The cell nucleation density was determined by a method described previously[6] and is the number of bubbles that nucleated in each cm^3 of unfoamed polymer. The volume fraction of the bubbles was taken to be the area fraction of the bubbles in a micrograph as suggested by Underwood[13]. The density of each sample was determined by the weight displacement method, ASTM D792.

RESULTS AND DISCUSSION

The solubility and diffusivity of CO_2 in ABS

Figure 1 shows the gas sorption of CO_2 into 1.5 mm thick ABS sheet subjected to saturation pressures of 350 kPa, 1 MPa, 2 MPa, 3 MPa, 4 MPa, 5 MPa, and 6 MPa at a saturation temperature of 26.7°C (80°F). The CO_2 concentration in mg gas/g polymer is plotted vs time. Over time, the concentration of CO_2 increases within the polymer until the polymer absorbs no more gas and can be considered saturated. As expected, the concentration of gas at equilibrium increases as the saturation pressure is increased. For the ABS formulation studied here, equilibrium concentrations as high as 150 mg CO_2/g polymer were achieved at a saturation pressure of 6 MPa. Figure 1 also shows that the diffusion of CO_2 in ABS is

Figure 1 Sorption curves for 1.5 mm thick ABS in CO_2 at 26.7°C (80°F), and pressures ranging from 350 kPa to 6 MPa. Increasing saturation pressures result in short er saturation times and higher equilibrium concentrations
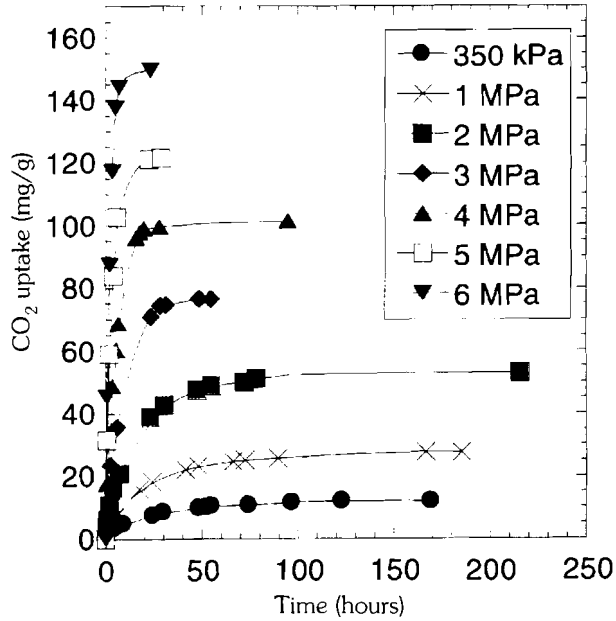
dependent on gas pressure. We see that it takes approximately 50 hours to reach equilibrium at a saturation pressure of 3 MPa, while at 6 MPa the equilibrium is reached in 20 hours. The faster diffusion at 6 MPa is a result of effective Tg of the gas-polymer system approaching the saturation temperature of 26.7°C. This is evident from Figure 5 where, for 6 MPa saturation, the onset of bubble nucleation is around 27°C.

The equilibrium concentration in milligrams of CO_2 per gram polymer is plotted in Figure 2 as a function of the saturation pressure. The set of points in Figure 2 define the sorption isotherm for 26.7°C. Usually this isotherm can be characterized using the Dual Mode Sorption Model[14]. In this system at 26.7°C however, a straight line passing through the origin represents all of the data accurately, and therefore Henry's Law can be used to predict the equilibrium concentration at a given saturation pressure:

$$C = H P_s \qquad (1)$$

where C is the equilibrium gas concentration, mg/g; H is Henry's Law constant (or solubility), mg/g·MPa; and Ps is the saturation pressure, MPa.

Figure 2 Sorption isotherm for CO_2 in ABS at 26.7°C (80°F). Note that equilibrium concentration increases linearly with saturation pressure and the linear regression passes through the origin, indicating Henry's Law is valid for a wide range of pressures in this system
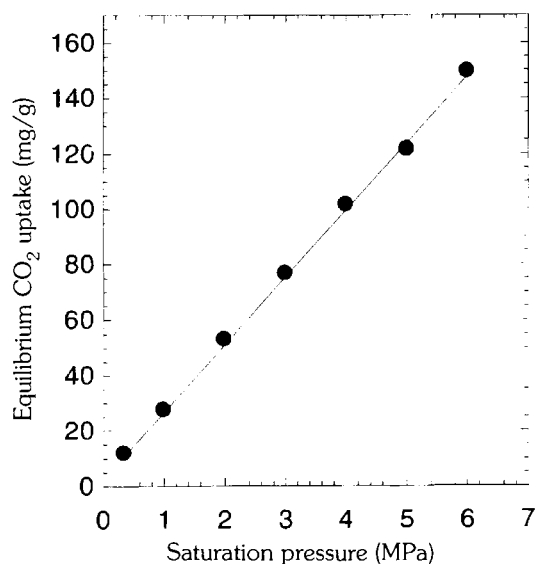

Figure 2 shows that Henry's Law is valid for all of the saturation pressures explored. From a least squares fit of the data in Figure 2, the Henry's Law constant was determined to be 25.0 mg/g·MPa for a saturation temperature of 26.7°C.

Figure 3 shows desorption results for ABS at 26.7°C, where the fraction of the gas remaining from the fully saturated condition is plotted as a function of time. The rate of desorption seen in Figure 5 is a function of the initial CO_2 concentration; increasing saturation pressure (or equivalently the equilibrium concentration) results in a faster rate of desorption. This behaviour is consistent with our observations from Figure 1 where higher saturation pressures led to significantly lower sorption times.

The average diffusion coefficient, D, can be estimated from Figure 1 using the solution of the diffusion equation for a plane sheet[15]. This diffusion coefficient is an average over the entire range of gas concentrations experienced by the sample, and is given by:

$$D = \frac{0.049}{\left(\dfrac{t}{l^2}\right)_{1/2}} \qquad (2)$$

Figure 3 Desorption curves for 1.5 mm ABS at 26.7°C and atmospheric conditions. The gas concentration is given as a fraction of the initial concentration. A higher initial saturation pressure results in a faster desorption
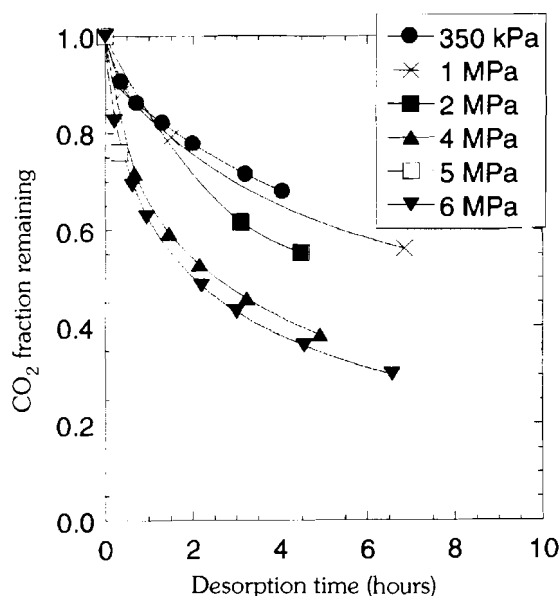
where t is the sorption time, l is the thickness of the sheet, and $(t/l^2)_{1/2}$ is the value of t/l^2 when half of the equilibrium amount of gas has been absorbed. Table 1 presents the approximate time to reach saturation, and the average diffusion coefficients for CO_2 in ABS for different gas pressures. We see that the diffusion coefficients range from 2.14×10^{-8} cm^2/sec for saturation at 350 kPa to 19.2×10^{-8} cm^2/sec at 6.0 MPa. As a result of this concentration dependent diffusivity, the saturation time decreases (see Table 1) with increasing saturation pressure, from about 120 hours at 350 kPa to about 8 hours at 6.0 MPa.

Table 1 Approximate saturation time to equilibrium, and sorption diffusion coefficient of CO_2 into 1.5 mm thick ABS sheet at 26.7° C

Saturation pressure (MPa)	Saturation time (hours)	Average diffusion coefficient $(cm^2$/sec$)$
0.350	120	2.14×10^{-8}
1.0	96	2.22×10^{-8}
2.0	72	2.46×10^{-8}
3.0	36	4.51×10^{-8}
4.0	24	7.81×10^{-8}
5.0	18	13.8×10^{-8}
6.0	8	19.2×10^{-8}

Conditions for steady-state structure

The objective of this portion of the study was to determine the foaming time required to produce ABS foams with a steady-state, or equilibrium, density. From the instant a saturated sample is placed in the glycerin bath, the bulk density of the specimen decreases at an ever decreasing rate until a steady sate value is achieved. After the foam density has reached steady-state, the density stops decreasing. For a given specimen thickness, the time required to reach steady-state is a function of the saturation pressure and temperature, and foaming temperature.

In this experiment, samples were saturated with CO_2 maintained at 350 kPa (50.8 psi) and 22°C, and foamed at 120°C for various lengths of time. The lowest gas pressure was chosen for this experiment so as to find the longest time needed to achieve steady-state structure. The foam density as a function of foaming time is plotted in Figure 4. Recall that the density of the original, unfoamed ABS was 1.04 g/cm^3. Figure 4 shows that it takes approximately 300 seconds (5 min) to reach steady-state in the ABS-CO_2 system for the given processing conditions. Since most other processing conditions will reach an equilibrium foam density faster than at these conditions, we used a foaming time of 300 seconds for all experiments in this study. In addition, Figure 4 shows that at a foaming temperature of 120°C, the original density is reduced by approximately 50% during the 300 seconds of foaming.

Figure 4 Plot of foam density as a function of foaming time, showing that a foaming time of approximately 300 seconds is required to reach equilibrium in the ABS-CO_2 system. Samples were saturated at 350 kPa, allowed to desorb for 5 minutes, then foamed at 120°C
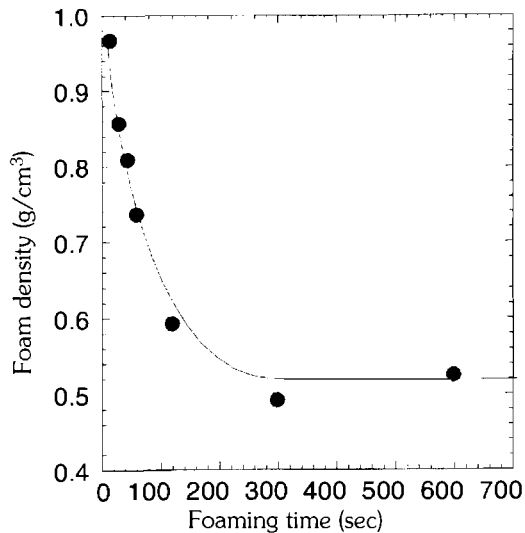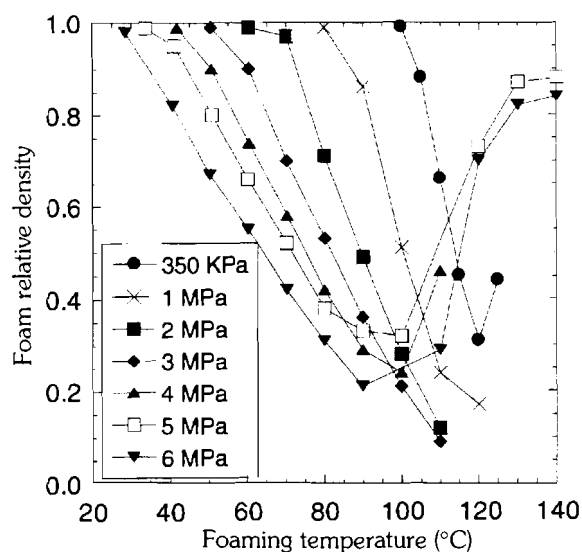
The effect of saturation pressure and foaming temperature

To explore the effect of foaming temperature and saturation pressure on microstructure, samples were saturated at different pressures and then foamed over a range of temperatures. After the samples had been produced, the foam density, average cell size, cell size distribution, and cell nucleation density were determined.

Figure 5 shows a plot of the relative density (density of the foam divided by the density of the solid material) as a function of foaming temperature for the saturation pressures explored. A wide range of relative densities can be produced in the ABS-CO_2 system. Foams can be produced with relative densities from 0.99 (i.e. almost fully dense) to as low as 0.09. In addition, most densities can be produced by using more than one processing condition. In other words, different saturation conditions and foaming temperatures can be used to produce the same density foam. Similar to other microcellular systems, Figure 5 shows that foaming can occur in ABS at temperatures significantly below the glass transition temperature of the unsaturated material due to plasticizing of the polymer matrix by the absorbed CO_2. As the saturation pressure is increased, the effective glass transition temperature drops, allowing foams to be produced

Figure 5 Process space for the ABS-CO_2 system, showing a plot of the relative density as a function of foaming temperature for saturation pressures from 350 kPa to 6 MPa. All samples were saturated at 26.7°C, allowed to desorb for five minutes before foaming, then foamed for five minutes. The useful part of the process space lies to the left of the minimum density for a given gas pressure

at lower temperatures. At a saturation pressure of 6 MPa, Figure 5 shows that foaming is possible at approximately 27°C, just above room temperature.

The relative density of microcellular ABS is affected strongly by the foaming temperature. As the foaming temperature increases, the relative density decreases in near linear proportion. The fact that relative density decreases nearly linearly with foaming temperature is a great processing advantage, allowing precise control over this vital foam property. As the foaming temperature increases, the foam density reaches a minimum, and can start to increase with increasing temperature. At 5 MPa, Figure 5 shows that using foaming temperatures higher than 100°C produces foams with a higher relative density. At 140°C, for example, a relative density of approximately 0.8 is produced, significantly higher than the relative density of 0.3 produced at a foaming temperature of 100°C. At higher temperature, the cells begin to collapse leading to a denser structure. Foams produced at these higher temperatures are typically of poor quality, with 1 to 2 mm blisters on the surface. This minimum in the density versus foaming temperature can be observed at several other gas pressures in Figure 5.

Figure 6 shows SEMs of four different microcellular ABS foams. The first two images, A and B, demonstrate the large effect of saturation pressure on foam density and cell size. Figure 6 A and B were produced with different saturation pressures, 3 and 6 MPa respectively, but the same foaming temperature of 70°C. The foams in A and B have relative densities of 0.70 and 0.42 respectively. The cell sizes vary from approximately 5 μm for A to less than 1 μm for B. Images C and D in Figure 6 show two foams produced from the same saturation pressure, 350 kPa, but foamed at different temperatures, 105 and 120°C. The foams have relative densities of 0.88 for C and 0.31 for D and show markedly different foam structures.

Table 2 presents the results of the scanning electron micrograph analysis, and shows it is possible to produce microcellular ABS foams with a wide range of cellular properties. Not all foams were suitable for analysis using Saltikov's method. To be suitable for analysis, the foam structure should have spherical cells, and the cells must be distinct in the micrograph. For example, in Figure 6 images A and C can be analyzed, while B and D can not. Thus the test pressures and foaming temperatures not reported in Table 2 are the conditions that produced cells not suitable for a Saltikov analysis. The measured average cell diameters in Table 2 vary from 5.58 μm to 0.54 μm, and the cell nucleation density ranges from 4.0×10^{10} to 1.8×10^{13} cells per cm^3. Microcellular ABS foams generally have small cell sizes and high cell nucleation densities.

Figure 6 Micrographs of four different microcellular ABS foams. A and B were saturated at different pressures, 3 MPa and 6 MPa respectively, but were foamed at the same temperature, 70°C. C and D were both saturated at the same pressure, 350 kPa, but were foamed at different temperatures, 105 and 120°C, respectively. All samples were allowed to desorb for five minutes before being foamed for five minutes
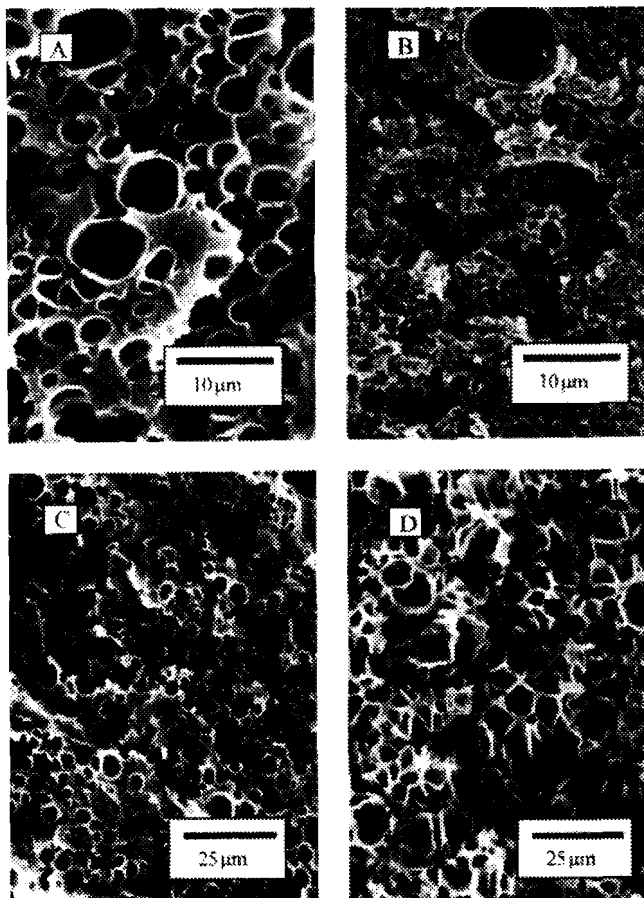
CONCLUSIONS

Processing conditions have been presented for producing solid-state microcellular ABS foams using carbon dioxide as the blowing agent. It was found that, at a given temperature, the rate of CO_2 sorption and desorption in ABS is dependent on the gas concentration. It was also discovered that the ABS-CO_2 system exhibited a unique microstructure with a relatively narrow distribution of bubble sizes. An experimental

Table 2 Foam characteristics and processing conditions for microcellular ABS foams

Saturation pressure (MPa)	Foaming temperature (° C)	Cell diameter			Cell nucleation density (cells/cm^3)
		Relative density	Average (μm)	Standard deviation (μm)	
0.350	105.0	0.88	2.39	0.90	2.7 x 10^{11}
0.350	110.0	0.66	3.32	1.06	2.2 x 10^{11}
0.350	115.0	0.45	4.57	1.50	1.8 x 10^{11}
1.0	90.0	0.86	1.65	0.61	9.8 x 10^{11}
1.0	100.0	0.51	2.86	1.13	8.2 x 10^{11}
2.0	70.0	0.97	0.94	0.54	4.7 x 10^{11}
2.0	80.0	0.71	2.60	1.03	3.6 x 10^{11}
2.0	90.0	0.49	3.78	1.29	2.3 x 10^{11}
3.0	60.3	0.90	3.58	0.83	4.0 x 10^{10}
3.0	70.2	0.70	2.21	0.90	5.3 x 10^{11}
3.0	80.0	0.53	4.43	1.32	1.1 x 10^{11}
3.0	90.0	0.36	5.58	2.58	6.8 x 10^{10}
4.0	60.0	0.77	0.50	0.22	1.8 x 10^{13}
4.0	80.0	0.45	4.14	1.81	8.8 x 10^{10}
4.0	100.0	0.17	4.21	2.08	5.9 x 10^{10}
5.0	80.0	0.38	0.54	0.27	1.4 x 10^{13}
5.0	100.0	0.28	1.14	0.48	1.4 x 10^{12}

investigation of the major processing variables, foaming time, saturation pressure, and foaming temperature yielded several insights into the processing behaviour of the ABS-CO$_2$ system. It was determined that it takes a maximum of approximately 300 seconds for foam growth to complete. It was also determined that, for all saturation pressures explored, foam density decreases nearly linearly with increasing foaming temperature until a minimum density is reached. Foams with densities ranging from 0.09 g/cm^3 to almost fully dense, 1.03 g/cm^3 were produced. The useful range of process space for the ABS-CO$_2$ system was established.

ACKNOWLEDGEMENTS

REFERENCES

1. Brisimitzakis A.C., Styrenic resins - ABS, Modern Plastics, **68**, (1991), 85-86

2. Martini J.E., Suh N.P. and Waldman F.A., The Production and Analysis of Microcellular Thermoplastic Foams, Society of Plastics Engineers Technical Papers, XXVIII, (1982), 674-676

3. Kumar V. and Schirmer H.G., Semi-Continuous Production of Solid State PET Foams, Society of Plastics Engineers Technical papers, **XLI**, (1995), 2189-2192

4. Kumar V. and Schirmer H.G., A Semi-Continuous Process to Produce Microcellular Foams, US Patent 5,684,055 (1997)

5. Kumar V. and Weller J.E., A Model for the Unfoamed Skin on Microcellular Foams, Polymer Engineering and Science, **34**, (1994), 169-173

6. Kumar V. and Weller J.E., Production of Microcellular Polycarbonate Using Carbon Dioxide for Bubble Nucleation, Journal of Engineering for Industry, **116**, (1994), 413-420

7. Handa V.P., Wong B., Zhang Z., Kumar V., Eddy S. and Khemani K., Some Thermodynamic and Kinetic Properties of the System PETG-CO_2, and Morphological Characteristics of the CO_2-Blown PETG Foams, Polymer Engineering and Science, **39**, (1999), 55-61

8. Kumar V. and Stolarczuk P.J., Microcellular PET Foams produced by the Solid State Process, Society of Plastics Engineers Technical Papers, **XLII**, (1996), 1894-1899

9. Kumar V. and Weller J.E., A Process to Produce Microcellular PVC, International Polymer Processing, **7**, (1993), 73-80

10. Shimbo M., Baldwin D.F. and Suh N.P., Polym. Eng. Sci., **35**, (1995), 1387

11. Park C.B. and Suh N.P., Polym. Eng. Sci., **36**, (1996), 34

12. Collias D.I., Baird D.G. and Borggreve R.J.M., Polymer, **25**, (1994), 3978

13. Underwood E.E., Quantitative Stereology, Adison-Wesley, Reading, Massachusetts, (1970)

14. Michaels A.S., Vieth W.R. and Barrie J.A., Solution of Gases in Polyethylene Terephthalate, Journal of Applied Physics, **34**, (1963), 1-12

15. Crank J., The Mathematics of Diffusion, Oxford University Press, New York (1975)